ACS Catalysis

Research Article

pubs.acs.org/acscatalysis

Electrocatalytic Oxygen Evolution Reaction (OER) on Ru, Ir, and Pt Catalysts: A Comparative Study of Nanoparticles and Bulk Materials

Tobias Reier,* Mehtap Oezaslan, and Peter Strasser

The Electrochemical Energy, Catalysis, and Materials Science Laboratory, Technische Universität Berlin, Department of Chemistry, 10623 Berlin, Germany

ABSTRACT: A comparative investigation was performed to examine the intrinsic catalytic activity and durability of carbon supported Ru, Ir, and Pt nanoparticles and corresponding bulk materials for the electrocatalytic oxygen evolution reaction (OER). The electrochemical surface characteristics of nanoparticles and bulk materials were studied by surface-sensitive cyclic voltammetry. Although basically similar voltammetric features were observed for nanoparticles and bulk materials of each metal, some differences were uncovered highlighting the changes in oxidation chemistry. On the basis of the electrochemical results, we demonstrated that Ru nanoparticles show lower passivation potentials compared to bulk Ru material. Ir nanoparticles completely lost their voltammetric metallic features during the voltage cycling, in contrast to the corresponding bulk material. Finally, Pt nanoparticles show an increased oxophilic nature compared to bulk Pt. With regard to the OER performance, the most pronounced effects of nanoscaling were identified for Ru and Pt catalysts. In particular, the Ru nanoparticles suffered from strong corrosion at applied OER potentials and were therefore unable to sustain the OER. The Pt nanoparticles exhibited a lower OER activity from the beginning on and were completely deactivated during the applied OER stability protocol, in contrast to the corresponding bulk Pt catalyst. We highlight that the OER activity and durability were comparable for Ir nanoparticles and bulk materials. Thus, Ir nanoparticles provide a high potential as nanoscaled OER catalyst.

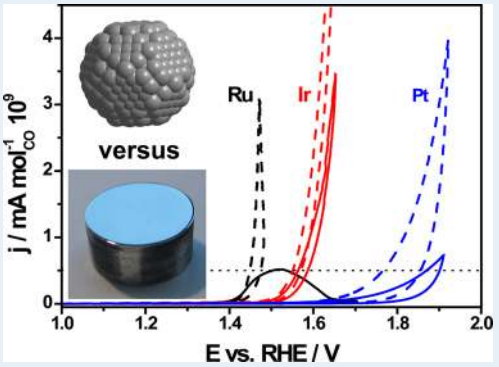

KEYWORDS: *oxygen evolution reaction (OER), water splitting, iridium, ruthenium, platinum, anodic oxidation, nanoparticles*

1. INTRODUCTION

One major roadblock on the way to a sustainable energy infrastructure based on renewable energies is an appropriate grid-scale chemical energy storage solution. A grid scale energy storage solution is constituted by the electrocatalytic splitting of water into molecular hydrogen and oxygen using polymer electrolyte membrane (PEM) electrolyzer architectures. Considering the cathodic part of water splitting, that is, the reduction of water to hydrogen, Pt is a nearly ideal catalyst.[1,2] In contrast, for the anodic part, that is, the oxidation of water to molecular oxygen in strong acidic environment (referred to as oxygen evolution reaction (OER)), the search of active, stable, and inexpensive electrocatalysts is an outstanding problem to date.[3]

Although, the OER itself has been described as early as 1789, detailed molecular insight into the relationship between catalyst surface structure and OER reactivity has remained scarce.[3,4] Thermochemical density functional theory (DFT)-based OER studies have predicted the binding energy of a surface oxygen species as the activity-controlling parameter, yielding a volcano type activity plot, with Ru and Ir oxide near the top.[5,6] Furthermore, alloys of Ru and Ir with other transition metals showed improved OER activity, as reported by Neyerlin and Forgie.[7,8] Amorphous oxide catalysts, such as RuO_x, revealed an increased OER performance compared to crystalline Ru oxide catalysts, because of an enhanced structural flexibility,[9] but showed insufficient durability.[10,11]

Ru and Ir oxides have emerged as the most promising catalyst candidates for the OER and thus are frequently studied.[12−15] Active and stable non-noble metal based catalysts for the OER in acidic media are essentially unknown because of the acid-aggressive and strong corrosive conditions. Recent research has therefore focused on the reduction of the noble metal amount in PEM electrolyzers, for example by using supported metal (oxide) nanoparticles and mesoporous metal oxide films.[16−19] Nanoscale catalysts are of great advantage because of the reduced noble metal content and a high catalytically active surface area achieved by a large surface area to volume ratio.[20] On the other hand, the choice of an appropriate corrosion-resistant support for the OER is a further challenge. Commonly used conductive carbon support materials, such as carbon nanotubes or carbon blacks, show stability deficiencies at high potentials which constrain their utilization in OER catalysis.[21] The stability of carbon based support materials can be improved by graphitization or carbide formation.[22−24] For example, TiC has proved to be a promising

Received: January 6, 2012
Revised: July 9, 2012
Published: July 23, 2012

   dx.doi.org/10.1021/cs3003098 | ACS Catal. 2012, 2, 1765−1772

candidate as support material for the OER with improved high voltage stability.[16]

Nevertheless, supporting and nanoscaling of OER anode electrocatalysts are in their early research stages. Although the effects of nanoscaling of OER catalysts, such as catalyst−support-interactions and particle size effects, can have great impact for both activity and stability,[25,26] they are scarcely studied. For instance, unsupported crystalline RuO_2 reported by Jirkovský et al. showed an improved OER activity with decreasing particle size.[27,28] This activity improvement was explained by the availability of certain edge atoms. In a Tafel analysis of RuO_2, the rate determining step (rds) for the OER was related to the crystallite size. Large crystals showed a similar rds as single crystals.[29] However, systematic OER studies focusing on the effects of nanoscaling and supporting of different OER electrocatalysts, are missing to date.

Here, we present an investigation of various nanoscaled OER electrocatalysts (Ru, Ir, and Pt) to reveal trends for the catalytic performance and stability. We compare the electrochemical characteristics and the resulting OER activities and stabilities for electrochemically oxidized metal nanoparticles of Ru, Ir, and Pt with those for the corresponding bulk metal catalysts as benchmarks. We find the OER activity to be sensitively dependent on the dimension of the Ir, Ru, and Pt catalysts. On the basis of electrocatalytic results, distinct activity and stability trends for each noble metal are uncovered.

2. EXPERIMENTAL SECTION

2.1. Synthesis of Carbon Supported Nanoparticles. Ru and Ir nanoparticles supported on Vulcan XC 72R with a metal loading of 20 wt % were synthesized by an incipient wetness method. Vulcan XC 72R (240 mg, GP-3875, Cabot) was impregnated with the appropriate amount of iridium acetate (48.76 wt % Ir, Heraeus, CAS#52705-52-9, LOT#10307) or ruthenium acetate (42.23 wt % Ru, Heraeus, CAS#55466−76−7, LOT#10309) which had previously been dissolved in 3.5 mL of deionized water (18 MOhm cm at room temperature). After careful horn-sonification, the impregnated powders were frozen in liquid nitrogen and freeze-dried in vacuum. Finally, the dried powders were annealed in a tube furnace under reductive atmosphere (4 Vol. % H_2, 96 Vol. % Ar, Air Liquide, quality 5.0). The furnace temperature was raised to 250 °C with a heating rate of 10 K/min and then to 465 °C with the maximal rate holding each temperature for 2 h. Commercially available Pt nanoparticles supported on Vulcan XC 72R (BASF Fuel Cell Inc.) with a loading of 20 wt % were used as received.

2.2. Electrode Preparation. Supported metal nanoparticle catalysts were coated as thin film layer on a previously polished and cleaned glassy carbon surface of a rotating disk electrode (RDE) (5 mm diameter, Pine Research Instrumentation). Therefore, a catalyst ink was prepared by mixing of the catalyst powder (5.00 mg), deionized water (3.980 mL), 2-propanol (1.000 mL), and Nafion solution (20.0 μL, 5 wt % in lower aliphatic alcohols and H_2O, Sigma-Aldrich). The catalyst suspension was horn-sonificated for 10 min. Ten microliters of the catalyst ink were pipette onto the glassy carbon surface and dried for 10 min at 60 °C in air to form a homogeneous, thin film.

Bulk ruthenium (American Elements, purity 99.95%) and iridium (MaTec, purity 99.99%) catalysts, cylinders with a diameter of 5 mm, were fixed on a Teflon interchangeable RDE holder (Pine Research Instrumentation). Platinum (Pine Research Instrumentation, purity 99.99%) was permanently embedded in a polyether ether ketone RDE. Before each experiment, the bulk materials were carefully polished to a mirror like surface finish using diamond pastes (Buehler) down to 1 μm.

2.3. Electrochemical Measurements. All electrochemical measurements were performed in a RDE setup equipped with a three compartment electrochemical glass cell with Luggin capillary, PINE rotator (Pine Research Instrumentation) and potentiostat, VSP-5 or SP-200 (BioLogic, France). A saturated mercury/mercury sulfate (MMS) electrode was used as reference electrode. The reference electrode was calibrated against a reversible hydrogen electrode (RHE) in the same electrolyte at room temperature. All potentials were converted and referred to the RHE. The acid electrolyte solutions, 0.1 M $HClO_4$ and 0.05 M H_2SO_4, were prepared by diluting from a 70% perchloric acid (Sigma-Aldrich, 99.999%) and a 98% sulfuric acid (Carl Roth) with deionized water (18 MOhm cm at room temperature).

2.3.1. Electrochemical Surface Characterization Protocol. This protocol was only used for Ir and Ru catalysts to trace the potential-dependent behavior of irreversible oxide formation. The catalysts used for this protocol were rejected afterward and were not used for the OER study. The catalysts were immersed into the electrolyte at 0.05 V before the cyclic voltammogram measurement with a scan rate of 500 mV/s was started. The lower potential limit was kept constant at 0.05 V, whereas the upper potential limit was successively raised from 0.5 to 1.3 V with an increment of 0.1 V after each 100 cycles. In case of Ru catalysts, 100 scans with 500 mV/s were followed by 6 scans with 50 mV/s.

2.3.2. Determination of Surface Sites. The following electrochemical protocol was used for the determination of the electrochemically available surface sites for all electrocatalysts prior to the OER. Perchloric acid was used as electrolyte for Pt and Ru catalysts. Because of stability problems of perchloric acid at potentials below 1.0 V, sulfuric acid was used as electrolyte for Ir catalysts. Prior the electrochemical measurement, the working electrode was immersed under potential control at 0.05 V into the nitrogen-deaerated (15 min) electrolyte. The potential was cycled in the range of 0.05 and 1.0 V (0.8 V for Ir). After an electrochemical cleaning step (100 cycles with 500 mV/s), the scan rate was reduced to 50 mV/s. The number of surface sites for each catalyst was established with CO stripping. In the CO stripping experiments, the electrolyte was consecutively bubbled with CO and N_2 for 15 min, respectively, while the electrode remained at 0.05 V. The potential was then cycled from 0.05 V to x, with v to strip off the adsorbed CO completely (v = 20 mV/s, x = 1 V for Ru and Pt and v = 50 mV/s and x = 1.2 V for Ir). The CO stripping charge was corrected with the oxide formation charge in the same potential range without adsorbed CO and divided by two to gain the number of surface sites.[30]

2.3.3. Electrocatalytic OER Protocol. After the number of surface sites had been determined (2.3.2), the OER protocol was started. All measurements were conducted with 1600 rpm in 0.1 M $HClO_4$ at room temperature. The Ir catalysts were cleaned with water and transferred to $HClO_4$ for the OER experiment. To determine the OER performance, all Ru, Ir, and Pt catalysts were subjected to 1.0 V for 3 min, followed by a quasi stationary scan with 6 mV/s. The OER stability protocol, which subsequently took place after the OER activity protocol, consisted of 51 fast scans with 200 mV/s and one additional quasi stationary scan with 6 mV/s into the voltage range of the

dx.doi.org/10.1021/cs3003098 | ACS Catal. 2012, 2, 1765−1772

OER. The electrolyte resistance was measured by means of potentiostatic impedance prior to the OER measurement.

2.4. X-ray Diffraction. XRD profiles were measured in Bragg−Brentano geometry in a D8 Advance X-ray diffractometer (Bruker AXS) using a Cu Kα source, variable divergence slit, and position sensitive device as detector. Data were collected in a 2Θ range of 15° to 100° with an increment of 0.05°, a measuring time of 7 s per step, and a sample rotation rate of 15 rotations per minute. The XRD profiles were fitted with the Pearson VII function using the software Jade 8 (Materials Data Inc.). A corundum reference sample (Bruker AXS) was measured to determine instrumental line broadening. The full width at half-maximum (fwhm) of Bragg reflexes, corrected with the instrumental line broadening, was used to determine the crystallite size utilizing the Scherrer equation. A value of 0.9 was used for the Scherrer constant.[31,32]

2.5. Transmission Electron Microscopy. TEM micrographs were aquired using a FEI TECNAI G^2 20 S-TWIN equipped with LaB_6 cathode and GATAN MS794 P CCD camera. The microscope was operated at an acceleration voltage of 200 kV. The catalyst powders were suspended in a 1:1 mixture of 2-propanol and deionized water. The suspensions were pipetted onto a carbon coated copper grid (400 mesh, Plano). Particle size distributions were determined by counting of more than 250 particles using the ImageJ 1.43 software (U.S. National Institutes of Health).

2.6. ICP-OES. An inductively coupled plasma optical emission spectrometer (715-ES ICP, Varian) was employed to analyze the electrolyte after the OER protocol. The following emission lines were used: for Ru, 240.27 and 267.87 nm; for Ir, 212.68 and 224.27 nm; and for Pt, 203.65 and 224.52 nm.

3. RESULTS AND DISCUSSION

3.1. Nanoparticle Synthesis and Characterization. Ir and Ru nanoparticles supported on Vulcan XC 72R were synthesized by an acetate precursor-based incipient wetness-impregnation method. Because of the thermally well-decomposable precursor salts, this synthesis route yields surfactant-free carbon supported metal nanoparticles.

The X-ray diffraction data of the supported metal nanoparticles are shown in Figure 1. The broad reflections exhibit small crystallite sizes for Pt, Ir, and Ru nanoparticles. The reflections of Ru nanoparticles indicate a hexagonal crystal phase, whereas Ir and Pt nanoparticles show cubic phases. Because of the overlap by the very broad, amorphous background of the carbon support, Vulcan XC 72R, in the 2 Θ range between 20° and 50°, the mean crystallite sizes were evaluated from reflexes in the 50°−100° 2 Θ range (see Table 1). The line broadening analysis revealed a mean crystallite size

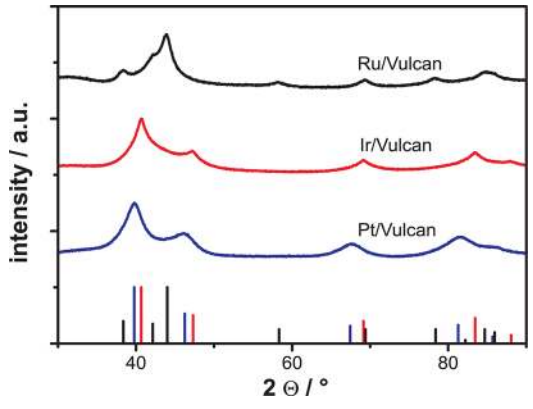

Figure 1. XRD patterns of Vulcan XC 72R supported Ru, Ir, and Pt nanoparticles. Vertical lines denote reference patterns taken from the powder diffraction file (PDF) of the international center of diffraction data, reference numbers Ru: 00-006-0663, Ir: 00-006-0598, Pt: 00-004-0802.

Table 1. Results of Particle Size Investigation for Vulcan XC 72R Supported Ru, Ir, and Pt Nanoparticles from TEM and XRD Line Broadening Analysis

nanocatalyst	particle size (TEM)/nm	crystallite size (XRD)/nm
Ru	4.3 ± 1.2	5.0 ± 0.3
Ir	2.0 ± 1.1	3.0 ± 0.1
Pt	2.5 ± 0.3	2.6 ± 0.1

of 5.0 ± 0.3 nm for Ru, 3.0 ± 0.1 nm for Ir, and 2.6 ± 0.1 mn for Pt, respectively. Energy dispersive X-ray measurements of Ru, Ir, and Pt nanocatalysts just showed the desired metals beside components of Vulcan XC 72R. Additionally, the mean particle size was determined from TEM images (see Figure 2).

The TEM images of the carbon-supported Ru, Ir, and Pt nanoparticles are presented in Figure 2. The nanoparticles were well distributed on the carbon support and exhibited mostly spherical shape. The evaluated particles size histograms showed a near logarithmic normal distribution which is common for nanocrystalline samples.[33] A detailed TEM investigation of the Pt nanoparticles used in this study is given in reference 24. The mean particle sizes (d_{avg} TEM) of all three metals, summarized in Table 1, are consistent with the XRD line broadening analysis. The slightly larger crystallite sizes established by XRD are due to the different types of averaging. The TEM analysis yields a number-average, whereas the XRD analysis yields a volume-average size.[32]

3.2. Electrochemical Surface Characterization. The electrochemical behavior and change of the surface oxidation states for Ru, Ir, and Pt catalysts were studied by recording of cyclic voltammograms (CVs).

3.2.1. Ruthenium-Nanoparticle and Bulk Electrocatalysts. Figure 3 shows selected CVs for Ru with an upper potential limit at and above 1.1 V highlighting the main features, differences, and similarities of Ru in the form of nanoparticles and bulk material. It is noted that Figure 3 reveals mostly featureless CVs without distinct current peaks for both Ru nanoparticle and bulk catalysts proving a basically similar electrochemical behavior. In the applied voltage range, Ru exists as Ru(III) below 0.8 V and as Ru(IV) above.[34,35] The observed increased current densities close to the turning potentials can be described by the highly irreversible nature of the oxidation and reduction processes of Ru. Exceeding a certain potential limit, these increased current densities diminished, and a new redox peak couple emerged at approximately 0.75 V, denoted as passivation. Considering the required potential limit for the passivation, the nanoparticle and bulk catalysts revealed a difference. The Ru nanoparticle catalyst already passivated exceeding potentials of 1.1 V as opposed to the bulk catalyst which passivated exceeding potentials of 1.2 V. The passivation process can be explained by the gradual conversion of Ru(IV) surface oxide species to an anhydrous RuO_2 oxide layer.[34,35] The observed surface chemistry of polycrystalline Ru is rather unique compared with other Pt group metals and deviates significantly from the surface chemistry of Ru (0001) single

dx.doi.org/10.1021/cs3003098 | ACS Catal. 2012, 2, 1765−1772

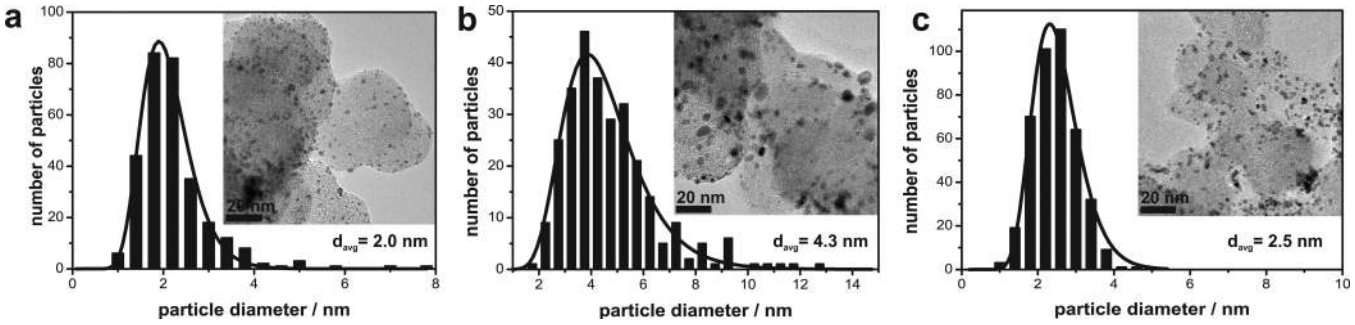

Figure 2. Bright field transmission electron micrographs and particle size distribution histograms of Ir (a), Ru (b), and Pt (c) nanoparticles supported on Vulcan XC 72R.

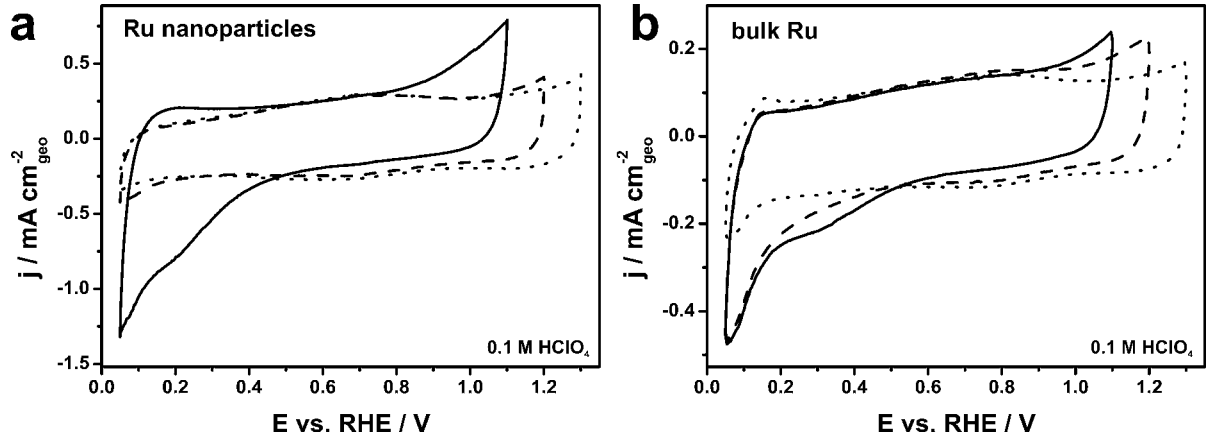

Figure 3. CVs of nanoparticle (a) and bulk (b) catalysts of Ru measured with 50 mV/s in deaerated 0.1 M $HClO_4$ at room temperature (RT). The upper potential limit was successively raised in 100 mV steps.

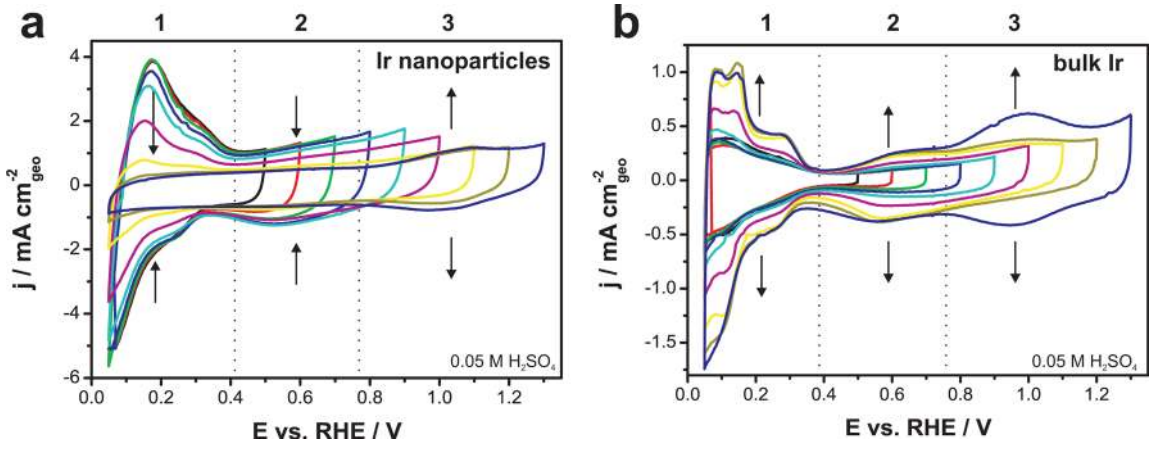

Figure 4. CVs of nanoparticle (a) and bulk (b) catalysts of Ir recorded with 500 mV/s in deaerated 0.05 M H_2SO_4 at RT. The upper potential limit was successively raised in 100 mV steps from 0.5 to 1.3 V. Each scan is number 100 in the given voltage range. Arrows indicate the increase or decrease of the three distinct regions by changing the upper turning potential.

crystals.[34−37] The Ru (0001) single crystal showed a distinct oxidation peak at 0.5 V and required one electron per surface atom for the oxidation processes prior to the oxidation of subsurface atoms.[37] In contrast the bulk Ru electrodes showed approximately 10 times larger oxidation currents and formed no distinct peaks yielding a featureless CV.[37] The absence of distinct hydrogen under potential deposition (Hupd) on polycrystalline Ru surfaces is likely based on the low voltage onset of oxide formation.[34,35,38]

3.2.2. Iridium-Nanoparticle and Bulk Electrocatalysts. Figure 4 shows a series of CVs for Ir nanoparticle and bulk catalysts. Here, the upper turning potential was successively increased from 0.5 to 1.3 V to monitor the changes of voltammetric features by the formation of irreversible surface oxide species. In contrast to Pt and Ru catalysts, the Ir catalyst was studied in a sulfuric acid electrolyte. It is well-known in the literature that perchloric acid is not suitable for low potential-iridium investigations because of the chemical instability of $HClO_4$ below 1.0 V, where perchlorate ions can be reduced in the presence of Ir catalysts to chloride ions.[39−41] Chloride ions have a strong tendency to bind on noble metal surfaces and thus strongly contaminate the surface.[42,43]

dx.doi.org/10.1021/cs3003098 | *ACS Catal.* 2012, 2, 1765−1772

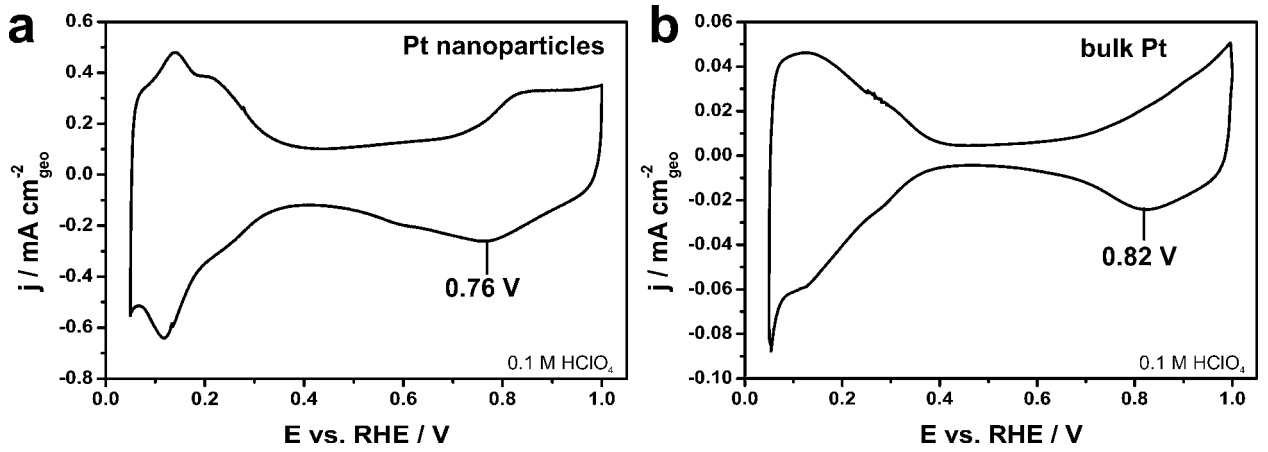

Figure 5. CVs of nanoparticle (a) and bulk (b) catalysts of Pt recorded with 50 mV/s in deaerated 0.1 M $HClO_4$ at RT.

The CVs shown in Figure 4a illustrate three main voltammetric features for Ir nanoparticles. Starting from low potentials, the CV profiles for Ir nanoparticles show a hydrogen adsorption region (1), distinguished by a large oxidation and reduction peak, followed by the formation of two different oxide species, each associated by a redox peak couple (2) and (3). Here, Ir was initially oxidized to an Ir(III) species as $Ir(OH)_3$ in the voltage region (2) and further to an hydrous Ir(IV) oxide species in the voltage region (3).[44]

Interestingly, when the anodic turning potential reached the voltage range for Ir(IV) oxide formation (3), both the Hupd (1) and the Ir(III) (2) formation peak started to decline until they had completely disappeared in the CV (Figure 4a). The current peak (3) growth and the decrease of the current peaks in region (1) and (2) evidence the electrochemical irreversibility of the Ir(IV) oxide formation. The disappearance of features, characteristic for metallic Ir, namely, the Hupd (1) and the oxide formation in voltage region (2), demonstrate the loss of the metallic character of the particle surface.

Bulk iridium catalysts show similarities to nanoparticle catalysts but also interesting differences (see Figure 44B). An interesting difference was observed in the voltage range of (3). Here, in contrast to the nanoparticles, the metallic features remained on the bulk Ir upon formation of Ir(IV) oxide and became more distinct.

Electrochemically formed Ir(IV) oxide layers are known to exhibit a porous structure which provides electrochemical access to the underlying metal, reported by Conway and Mozota.[45] Hence, in case of an Ir(IV) oxide covered bulk Ir catalyst the underlying metal can contribute to the voltammetric phenomena revealing the characteristic metallic features. The loss of the metallic nature of Ir nanoparticles initiated by continuous potential cycling between ranges (1) and (3), therefore, indicates the complete irreversible conversion of all Ir centers to Ir oxide species.

3.2.3. Platinum-Nanoparticle and Bulk Electrocatalysts. The CVs of Pt nanoparticle and bulk catalysts are compared in Figure 5. Both CVs exhibit the commonly characteristic features for pure Pt such as the Hupd region between 0.05 and 0.35 V, the double layer region commencing at 0.35 V, and the Pt (hydr-)oxide regime at and beyond approximately 0.7 V.[25] The direct comparison showed, however, some differences. In the view of the Pt-oxide reduction peak, a small cathodic peak shift is apparent for nanoparticles which is generally attributed to a particle size effect.[25] The chemical reason for this shift is based on the stronger adsorption behavior of oxygen on nanoparticles due to electronic and geometric effects.[25] Smaller particles offer a larger fraction of corner and edge atoms with low coordination numbers which bond oxygen stronger than terrace atoms with high coordination numbers.[26]

3.3. Electrocatalytic OER Activity and Stability. *3.3.1. Determination of Electrochemically Available Surface Sites.* The number of surface sites for Ru, Ir, and Pt catalysts were determined by CO stripping experiments and could subsequently be considered for the catalytic comparison of specific OER activities in acid. Here, the number of active surface sites was used to determine the specific current densities rather as the electrochemically active surface area, since this approach makes different surfaces with deviating density of active sites intrinsically comparable. Table 2 summarizes the number of electrochemically available surface sites for Pt, Ir, and Ru catalysts in the form of nanoparticles and bulk materials.

Table 2. Absolute Number of Surface Sites for Nanoparticle and Bulk Catalysts of Ru, Ir, and Pt Determined from CO Stripping Experiments

	number of active surface sites/10^{-9} mol	
catalyst	bulk	nanoparticles
Ru	4.50	5.54
Ir	0.45	3.26
Pt	0.40	3.38

Bulk Pt and Ir revealed comparable numbers of surface sites for bulk materials and nanoparticles. As expected, the number of electrochemically available surface sites was 7-fold higher for Ir and Pt nanoparticles than those for the corresponding bulk materials. In addition, the bulk Ru catalyst showed ten times more surface sites compared to Pt and bulk Ir catalysts. We hypothesized, that the bulk Ru catalyst was roughened during voltage cycling because of the low onset potential for oxide formation. Furthermore, the geometric current densities observed in the CVs for polycrystalline bulk Ru catalysts are known to be approximately 10 times higher than those for Ru (0001) single crystal electrodes.[37]

3.3.2. Specific OER Activity and Stability. In the following section the specific OER activities of all catalysts will be reported together with the stability study. Here, the specific current densities and specific OER activities were obtained by

dx.doi.org/10.1021/cs3003098 | ACS Catal. 2012, 2, 1765−1772

normalizing the current to the number of surface sites established by CO stripping experiments (see 3.3.1). All Ir, Ru, and Pt catalysts were tested for the OER in $HClO_4$. It is noted that the chemical instability of $HClO_4$ with respect to Ir is only relevant in the low voltage range which was not applied during this OER study. Figure 6 shows the specific OER

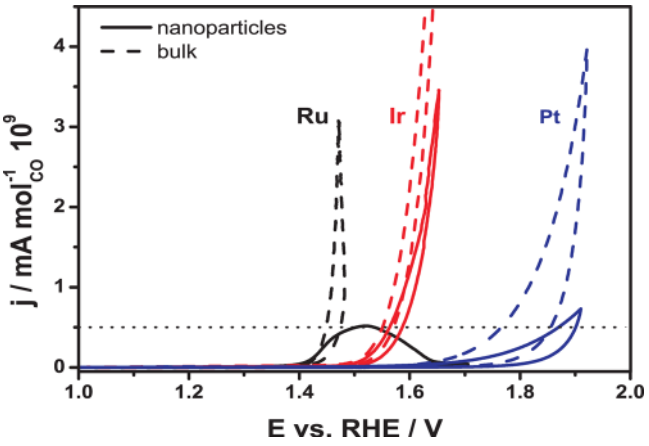

Figure 6. First quasi stationary OER scan for bulk and nanoparticle catalysts of Ru, Ir, and Pt recorded with 6 mV/s and 1600 rotations per minute (rpm) in deaerated 0.1 M $HClO_4$ at RT. The current is normalized to the number of surface sites determined from CO stripping experiments.

activities in terms of quasi-stationary cyclic polarization curves into the OER voltage region in 0.1 M $HClO_4$. To detect non-OER related anodic currents, which can be related to catalyst degradation processes or metal oxidation reactions, a series of polarization curves were performed as stability test. Subsequently, the used electrolyte was analyzed by inductively coupled plasma optical emission spectrometry (ICP-OES) to quantify the amount of dissolved metal from the tested catalyst. Here, the required overvoltage for a given specific OER current density serves as measure for the catalytic activity (see Figure 6 and Table 3).

The bulk Ru catalyst showed the best intrinsic OER activity in this study. Close to the OER onset potential, Ru nanoparticles revealed a comparable activity. But, in contrast to the bulk catalyst, a current maximum appeared during the first anodic scan, indicating stability problems for Ru nanoparticles. On the basis of the ICP analysis, the amount of dissolved Ru equaled the used total loading of metal nanocatalyst within the accuracy of the ICP measurement. So, the Ru nanoparticles were completely dissolved during the first anodic scan. Considering a maximum dissolution charge for Ru, by assuming the dissolution of Ru as RuO_4,[10,11] the calculated value could only account for 19% of the observed anodic charge. Because only one anodic current peak was observed, the dissolution process and the OER on Ru nanoparticles apparently took place in the same voltage range. This observation was corroborated by in situ reflectance measurements of bulk Ru catalysts which detected the formation of RuO_4 as corrosion product at the onset potential of the OER.[10] In the case of bulk Ru catalyst, the dissolution charge could account for maximal 4% of the anodic charge observed during the OER activity and stability protocol. Thereby, the nanoparticle catalyst revealed a larger fraction of dissolved Ru compared to the bulk catalyst. The instability of Ru nanocatalyst with a size of 4−6 nm may be explained by a higher surface energy of small particles which likely facilitates the electrochemical dissolution process.

In contrast to Ru catalyst, both nanoparticles and bulk catalysts of Ir showed stable polarization curves. Very similar OER activities were observed for Ir nanoparticles and bulk material. In addition, the OER activity remains almost unchanged during the applied OER stability test (not shown). The compositional stability was also supported by the ICP analysis of the electrolytes after the OER stability test. Only small amounts of dissolved Ir were found for the nanocatalyst, while no metal was detected for the bulk Ir catalyst (see Table 3). Unlike Ir nanoparticles, the bulk catalyst exhibited a significantly smaller surface area and therefore a reduced loss of metal. Interestingly, the activity of both Ir catalysts only deviated by 12 mV at 0.5 × 10^9 mA/mol. Further work is in progress to clarify the effect of particle size for Ir.

Turning to the Pt catalysts, the nanoparticles showed a significantly lower OER performance than the bulk material (see 7a). Furthermore, after the OER stability protocol the Pt nanocatalyst was completely deactivated, while the bulk catalyst only showed a reduced activity (see Figure 7a). To clarify the strong decay of performance, CVs for Pt nanoparticles were recorded before and after the OER stability test (see Figure 7b). Here, the CV revealed the commonly characteristic features for Pt after the OER stability test. Despite the complete deactivation for the OER, the CV (Figure 7b) indicated the electrochemical accessibility of Pt nanoparticles after the OER stability protocol. In accordance with this result, no Pt was detectable in the electrolyte after the OER stability test. Shown in Figure 7b, the reduced Hupd regime evidenced a loss of Pt surface area because of a catalyst degradation process. Moreover, the increased current density in the double layer region also indicated an alteration of the supporting material, connected to a gain of surface area. The catalyst degradation, however, cannot explain the complete deactivation for the OER.

To describe the lower activity of Pt nanoparticles compared to the bulk material a model developed by Damjanovic for bulk Pt catalysts was considered. Under potential conditions of the OER, the surface is covered with a poorly conductive Pt oxide species.[46,47] The electrons freed during the OER have to tunnel

Table 3. Potentials for an OER Current Density of 0.5 mA mol^{-1} 10^9, Tafel Slopes, and Dissolved Metal Masses for Ir, Ru, and Pt Nanoparticle and Bulk Catalysts

	potential at 0.5 mA mol^{-1} 10^9/V		Tafel slope/mV dec^{-1}		dissolved metal (ICP)/μg	
catalyst	bulk	nanoparticles	bulk	nanoparticles	bulk	nanoparticles
Ru	1.449	1.504	44		13.1 ± 0.2	1.7 ± 0.4
Ir	1.551	1.563	63	64	bld[a]	0.8 ± 0.3
Pt	1.766	1.870	145	210	bld[a]	bld[a]

[a]bld - below limit of detection.

dx.doi.org/10.1021/cs3003098 | ACS Catal. 2012, 2, 1765−1772

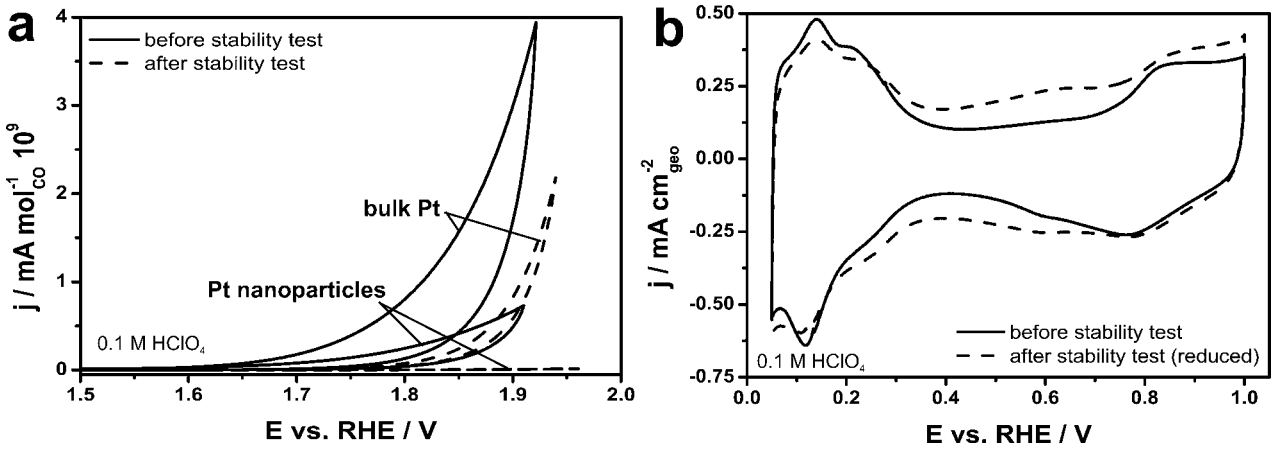

Figure 7. (a) Quasi stationary OER scans of nanoparticle and bulk catalysts of Pt before and after OER stability test measured with 6 mV/s and 1600 rpm in deaerated 0.1 M $HClO_4$ at RT. (b) CVs for Pt nanoparticles before and after OER stability test.

through this oxide layer which makes the current exponentially dependent on the oxide layer thickness at a certain electrode potential.[46] Because of the more pronounced oxophilicity of Pt nanoparticles compared to bulk material, the poorly conductive oxide layer may grow faster and become thicker on nanoparticles. With a thicker oxide layer, the current decreases which likely explains the lower activity of the Pt nanoparticles. The complete deactivation may be related to an almost complete oxidation of Pt nanoparticles.

The OER activity of Pt catalysts was the lowest in this study. This observation is exceptional because Pt is known as good catalyst for the reverse reaction, the reduction of molecular oxygen to water (ORR).[24,48] Moreover, a density functional theory (DFT) based study predicted for Pt oxide an OER activity comparable to or higher than that for Ir oxide dependent on the considered phase.[5]

3.3.3. Tafel Behavior. The Tafel behavior, especially the Tafel-slope, is an important kinetic parameter to reveal changes in the apparent OER mechanism.[49] Tafel-slopes determined from the data shown in Figure 6 are given in Table 3. The measured Tafel slope for the bulk Ru catalyst is in accordance with 41 mV/dec observed for a Ru electrode[50] and 39 mV/dec obtained for a thermally prepared RuO_2 electrode in sulphuric acid.[15] A Tafel-slope of 40 mV/dec is consistent with the second electron transfer step in the OER mechanism to be rate determining.[49] Because of the instability of Ru nanoparticles, a Tafel slope could not be determined.

Similar Tafel slopes of approximately 60 mV/dec were observed for nanoparticle and bulk catalysts of Ir, demonstrating that both catalysts exhibit the similar rate determining step for the OER. A value of 60 mV/dec can be indicative for a chemical rate determining step, in which an OH surface species is rearranged via a surface reaction.[49] The resulting Tafel-slopes for Ir deviated slightly from 55 mV/dec obtained for anodically oxidized Ir nanoparticles in sulphuric acid,[51] and are in good accordance with 61 mV/dec obtained for thermally prepared IrO_2 in sulphuric acid.[15]

Both Pt catalysts showed an exceptionally high Tafel slope, higher than 120 mV/dec found by Damjanovic.[46] A Tafel-slope above 120 mV/dec was not included in an OER mechanistic model.[49] The experimentally observed high Tafel-slope indicates additional contributions from processes with exponential current−potential dependency, probably related to the formation of Pt oxide layers.

4. CONCLUSIONS

A comparative study of the OER activity and stability for oxidized Ru, Ir, and Pt nanoparticle catalysts was presented and benchmarked to the corresponding bulk catalysts. The experimentally observed intrinsic OER activities for nanoparticle catalysts decreased in the order: oxidized Ru > oxidized Ir > oxidized Pt. Although the OER performance of Ru was outstanding, stability problems prevent the utilization of Ru nanoparticles as a practical nanoscaled OER catalyst. The Pt nanoparticles suffered from additional deactivation compared to the bulk catalyst and were therefore a suboptimal choice as a nanostructured OER catalyst. In this study, the supported Ir nanoparticles revealed a high activity and a sufficient stability for the OER. These findings point out that Ir nanoparticles emerge as a future nanoscaled OER catalyst concept for acidic PEM electrolyzer devices.

AUTHOR INFORMATION

Corresponding Author

*E-mail: tobias.reier@tu-berlin.de.

Funding

This project was supported by the Cluster of Excellence in Catalysis (unifying concepts in catalysis, UNICAT) funded by the DFG and managed by the TU Berlin.

Notes

The authors declare no competing financial interest.

ACKNOWLEDGMENTS

The authors thank Dr. rer. nat. Frédéric Hasché and the Central Facility for Electron microscopy at the Technische Universität Berlin for support.

REFERENCES

(1) Nørskov, J. K.; Christensen, C. H. *Science* **2006**, *312*, 1322−1323.
(2) Trasatti, S. *J. Electroanal. Chem. Interfacial Electrochem.* **1972**, *39*, 163−184.
(3) Dau, H.; Limberg, C.; Reier, T.; Risch, M.; Roggan, S.; Strasser, P. *ChemCatChem* **2010**, *2*, 724−761.
(4) de Levie, R. *J. Electroanal. Chem.* **1999**, *476*, 92−93.
(5) Man, I. C.; Su, H.-Y.; Calle-Vallejo, F.; Hansen, H. A.; Martínez, J. I.; Inoglu, N. G.; Kitchin, J.; Jaramillo, T. F.; Nørskov, J. K.; Rossmeisl, J. *ChemCatChem* **2011**, *3*, 1159−1165.
(6) Rossmeisl, J.; Qu, Z. W.; Zhu, H.; Kroes, G. J.; Nørskov, J. K. *J. Electroanal. Chem.* **2007**, *607*, 83−89.

(7) Neyerlin, K. C.; Bugosh, G.; Forgie, R.; Liu, Z.; Strasser, P. *J. Electrochem. Soc.* **2009**, *156*, B363−B369.
(8) Forgie, R.; Bugosh, G.; Neyerlin, K. C.; Liu, Z.; Strasser, P. *Electrochem. Solid-State Lett.* **2010**, *13*, B36−B39.
(9) Tsuji, E.; Imanishi, A.; Fukui, K.-i.; Nakato, Y. *Electrochim. Acta* **2011**, *56*, 2009−2016.
(10) Kötz, R.; Stucki, S.; Scherson, D.; Kolb, D. M. *J. Electroanal. Chem. Interfacial Electrochem.* **1984**, *172*, 211−219.
(11) Wohlfahrt-Mehrens, M.; Heitbaum, J. *J. Electroanal. Chem. Interfacial Electrochem.* **1987**, *237*, 251−260.
(12) Lodi, G.; Sivieri, E.; Battisti, A.; Trasatti, S. *J. Appl. Electrochem.* **1978**, *8*, 135−143.
(13) De Pauli, C. P.; Trasatti, S. *J. Electroanal. Chem.* **2002**, *538*−*539*, 145−151.
(14) Trasatti, S. *Electrochim. Acta* **1984**, *29*, 1503−1512.
(15) Mattos-Costa, F. I.; de Lima-Neto, P.; Machado, S. A. S.; Avaca, L. A. *Electrochim. Acta* **1998**, *44*, 1515−1523.
(16) Ma, L.; Sui, S.; Zhai, Y. *J. Power Sources* **2008**, *177*, 470−477.
(17) Ortel, E.; Reier, T.; Strasser, P.; Kraehnert, R. *Chem. Mater.* **2011**, *23*, 3201−3209.
(18) Sui, S.; Ma, L.; Zhai, Y. *Asia-Pac. J. Chem. Eng.* **2009**, *4*, 8−11.
(19) Nakagawa, T.; Beasley, C. A.; Murray, R. W. *J. Phys. Chem. C* **2009**, *113*, 12958−12961.
(20) Campelo, J. M.; Luna, D.; Luque, R.; Marinas, J. M.; Romero, A. A. *ChemSusChem* **2009**, *2*, 18−45.
(21) Maass, S.; Finsterwalder, F.; Frank, G.; Hartmann, R.; Merten, C. *J. Power Sources* **2008**, *176*, 444−451.
(22) Borchardt, L.; Hasché, F.; Lohe, M. R.; Oschatz, M.; Schmidt, F.; Kockrick, E.; Ziegler, C.; Lescouet, T.; Bachmatiuk, A.; Büchner, B.; Farrusseng, D.; Strasser, P.; Kaskel, S. *Carbon* **2012**, *50*, 1861−1870.
(23) Hasché, F.; Fellinger, T.-P.; Oezaslan, M.; Paraknowitsch, J. P.; Antonietti, M.; Strasser, P. *ChemCatChem* **2012**, *4*, 479−483.
(24) Hasché, F.; Oezaslan, M.; Strasser, P. *Phys. Chem. Chem. Phys.* **2010**, *12*, 15251−15258.
(25) Mayrhofer, K. J. J.; Blizanac, B. B.; Arenz, M.; Stamenkovic, V. R.; Ross, P. N.; Markovic, N. M. *J. Phys. Chem. B* **2005**, *109*, 14433−14440.
(26) Kinoshita, K. *J. Electrochem. Soc.* **1990**, *137*, 845−848.
(27) Jirkovský, J.; Hoffmannová, H.; Klementová, M.; Krtil, P. *J. Electrochem. Soc.* **2006**, *153*, E111−E118.
(28) Jirkovský, J.; Makarova, M.; Krtil, P. *Electrochem. Commun.* **2006**, *8*, 1417−1422.
(29) Guerrini, E.; Trasatti, S. *Russ. J. Electrochem.* **2006**, *42*, 1017−1025.
(30) Trasatti, S.; Petrii, O. A. *J. Electroanal. Chem.* **1992**, *327*, 353−376.
(31) Langford, J. I.; Wilson, A. J. C. *J. Appl. Crystallogr.* **1978**, *11*, 102−113.
(32) Cullity, B. D.; Stock, S. R. *Elements of X-Ray Diffraction*; Prentice Hall: Upper Saddle River, NJ, 2001; 385−402.
(33) Gubicza, J.; Szépvölgyi, J.; Mohai, I.; Zsoldos, L.; Ungár, T. *Mater. Sci. Eng., A* **2000**, *280*, 263−269.
(34) Juodkazytė, J.; Vilkauskaitė, R.; Šebeka, B.; Juodkazis, K. *Trans. Inst. Met. Finish.* **2007**, *85*, 194−201.
(35) Juodkazytė, J.; Vilkauskaitė, R.; Stalnionis, G.; Šebeka, B.; Juodkazis, K. *Electroanalysis* **2007**, *19*, 1093−1099.
(36) Vuković, M.; Čukman, D. *J. Electroanal. Chem.* **1999**, *474*, 167−173.
(37) Marinković, N. S.; Wang, J. X.; Zajonz, H.; Adžić, R. R. *J. Electroanal. Chem.* **2001**, *500*, 388−394.
(38) El-Aziz, A. M.; Kibler, L. A. *Electrochem. Commun.* **2002**, *4*, 866−870.
(39) Wasberg, M.; Horányi, G. *J. Electroanal. Chem.* **1995**, *385*, 63−70.
(40) Kaghazchi, P.; Simeone, F. C.; Soliman, K. A.; Kibler, L. A.; Jacob, T. *Faraday Discuss.* **2009**, *140*, 69−80.
(41) Pajkossy, T.; Kibler, L. A.; Kolb, D. M. *J. Electroanal. Chem.* **2007**, *600*, 113−118.
(42) Lam, A.; Li, H.; Zhang, S.; Wang, H.; Wilkinson, D. P.; Wessel, S.; Cheng, T. T. H. *J. Power Sources* **2012**, *205*, 235−238.
(43) Markovic, N.; Hanson, M.; McDougall, G.; Yeager, E. *J. Electroanal. Chem. Interfacial Electrochem.* **1986**, *214*, 555−566.
(44) Juodkazytė, J.; Šebeka, B.; Valsiunas, I.; Juodkazis, K. *Electroanalysis* **2005**, *17*, 947−952.
(45) Conway, B. E.; Mozota, J. *Electrochim. Acta* **1983**, *28*, 9−16.
(46) Damjanovic, A.; Birss, V. I.; Boudreaux, D. S. *J. Electrochem. Soc.* **1991**, *138*, 2549−2555.
(47) Schultze, J. W.; Vetter, K. J. *Electrochim. Acta* **1973**, *18*, 889−896.
(48) Hasché, F.; Oezaslan, M.; Strasser, P. *ChemPhysChem* **2012**, *13*, 828−834.
(49) Faria, L. A.; Boodts, J. F. C.; Trasatti, S. *J. Appl. Electrochem.* **1996**, *26*, 1195−1199.
(50) Miles, M. H.; Klaus, E. A.; Gunn, B. P.; Locker, J. R.; Serafin, W. E.; Srinivasan, S. *Electrochim. Acta* **1978**, *23*, 521−526.
(51) Pauporté, T.; Andolfatto, F.; Durand, R. *Electrochim. Acta* **1999**, *45*, 431−439.